

Circulation, dispersion and hydrodynamic connectivity over the Scotian Shelf and adjacent waters

Yi Sui¹, Jinyu Sheng^{1*}, Kyoko Ohashi¹ and Yongsheng Wu²

¹ Department of Oceanography, Dalhousie University, Halifax, Nova Scotia, B3H 4R2, Canada

² Ocean Ecosystem Sciences Division, Fisheries and Oceans Canada, Bedford Institute of Oceanography, Box 1006, Dartmouth, Nova Scotia, B2Y 4A2, Canada

Abstract: A nested-grid ocean circulation modelling system is used in this study to examine the circulation of surface waters over the Scotian Shelf and its adjacent coastal water bodies. The modelling system consists of a coarse-resolution (1/12°) barotropic storm surge (outer) model covering the northwest Atlantic Ocean, and a fine-resolution (1/16°) baroclinic (inner) model covering the Gulf of St. Lawrence, Scotian Shelf, and Gulf of Maine. The three-dimensional model currents are used to track trajectories of particles using a Lagrangian particle-tracking model. The simulated particle movements and distributions are used to examine the dispersion, retention, and hydrodynamic connectivity of surface waters over the study region. The near-surface dispersion is relatively high over western Cabot Strait, the inner Scotian Shelf, and the shelf break of the Scotian Shelf. The dispersion is relatively low in Northumberland Strait. A process study is conducted to examine the physical processes affecting the surface dispersion, including tidal forcing and local wind forcing. The model results show that the tidal currents significantly influence the dispersion of surface waters in the Bay of Fundy.

Keywords: circulation model; particle tracking; retention; dispersion; process study

*Correspondence to: Jinyu Sheng, Department of Oceanography, Dalhousie University, Halifax, Nova Scotia, B3H 4R2, Canada; Email: Jinyu.Sheng@Dal.Ca

Received: October 17, 2017; **Accepted:** December 8, 2017; **Published Online:** December 20, 2017

Citation: Sui Y, Sheng J, Ohashi K, *et al.* (2017). Circulation, dispersion and hydrodynamic connectivity over the Scotian Shelf and adjacent waters. *Satellite Oceanography and Meteorology*, 2(2): 321. <http://dx.doi.org/10.18063/SOM.v2i2.321>

1. Introduction

The eastern Canadian shelf (ECS) over the northwest Atlantic Ocean supports many ocean use sectors including commercial fisheries, aquaculture, offshore hydrocarbon production, shipping and transportation, marine recreation and tourism, and other economic activities that directly contribute to the Canadian economy (Rutherford *et al.*, 2005). This region also consists of several highly productive marine ecosystems such as rich commercial fishing grounds over the Grand Banks, Gulf of St. Lawrence (GSL), Scotian Shelf (SS) and Gulf of Maine (GoM).

Marine ecosystems are strongly influenced by physical environmental conditions such as ocean currents, temperature

and salinity. Ocean currents and turbulent mixing, for example, affect the availability of nutrients for plant growth and availability of food for marine animals. Eggs and larvae of fish and other animals, on the other hand, can drift with ocean currents from their spawning grounds to nursery areas where they feed and grow (Lauri, 1999).

Significant efforts have been made in the past to determine the general circulation and associated seasonal and interannual variability over the ECS (Smith and Schwing, 1991; Sheng and Thompson, 1996; Lynch *et al.*, 1996; Loder *et al.*, 1998; Wu *et al.*, 2012; Urrego-Blanco and Sheng, 2014a, b). The large-scale circulation over the ECS is predominantly influenced by the North Atlantic subpolar gyre and its western boundary current,

the Labrador Current (Loder *et al.*, 1998). The general circulation and hydrography over the ECS, particularly over the outer shelf and slope regions of the Scotian Shelf and Gulf of Maine, are also strongly affected by the western boundary current of the North Atlantic subtropical gyre, namely the Gulf Stream and its northern extension, the North Atlantic Current.

The three-dimensional (3D) currents, hydrographic conditions and particle movements on the ECS have significant temporal and spatial variability, which are affected by the local irregular bathymetry, tidal forcing, atmospheric forcing, and river discharge (Urrego-Blanco and Sheng, 2012). Cong *et al.*, (1996) calculated retention indices for offshore banks on the Scotian Shelf based on wind-driven currents produced by a barotropic circulation model. The particle movements over coastal embayments such as Halifax Harbour and Lunenburg Bay of the Scotian Shelf were calculated from 3D ocean currents produced by primitive-equation ocean circulation models (Sheng *et al.*, 2009; Shan *et al.*, 2012). Shan *et al.*, (2014) recently examined the 3D circulation and particle movement over Sable Gully of the Scotian Shelf. The main objective of this study is to examine the retention, dispersion, and hydrodynamic connectivity of passive particles in near-surface waters over the Scotian Shelf and its adjacent waters including the southern Gulf of St. Lawrence and inner Gulf of Marine using a Lagrangian particle tracking model with simulated 3D ocean currents.

The structure of the paper is as follows. Section 2 discusses the nested-grid coastal circulation modelling system and the Lagrangian particle tracking model. Section 3 discusses the performance of the circulation modelling system and the particle tracking model using three types of oceanographic observations. Section 4 discusses the calculated retention and dispersion of passive particles over the Scotian Shelf and adjacent waters. This section also examines the main physical processes affecting the surface dispersion. The last section presents the summary and conclusions.

2. Nested Grid Ocean Circulation Modeling System

2.1 Ocean Circulation Model

The ocean circulation model used in this study is a nested-grid ocean circulation modelling system known as DalCoast. The circulation modelling system is constructed from the Princeton Ocean Model (POM; Mellor, 2004), which is a 3D, sigma-coordinate, primitive-equation ocean circulation model. Different versions of DalCoast were

developed in the past for different scientific applications (Sheng *et al.*, 2009; Ohashi *et al.*, 2013; Shan *et al.*, 2012, 2014).

The version of DalCoast used in this study is very similar to that used by Ohashi and Sheng (2013, 2015) and has a nested two-level structure with a fine — resolution inner model nested inside a coarse-resolution outer model. The outer model domain covers the ECS from the Labrador Shelf (LS) to the Gulf of Maine (GoM) (72 °W–42 °W and 38 °N–60 °N) (Figure 1A). The inner model domain covers the GSL, the SS, the GoM, and adjacent deep waters (71.5 °W–56 °W and 38.5 °N–52 °N) (Figure 1B). The outer model is two-dimensional and barotropic with a horizontal resolution of 1/12 °. The inner model is baroclinic and three-dimensional with a horizontal resolution of 1/16 °. The inner model has 40 sigma (terrain-following) levels in the vertical that are concentrated near the surface and bottom. The model bathymetry is based on the General Bathymetric Chart of the Oceans (GEBCO) data with a resolution of 30 arc-seconds (Weatherall *et al.*, 2015).

The outer model is driven by atmospheric forcing. The inner model external forcing includes tidal forcing, atmospheric forcing, surface heat fluxes, and river discharge. The atmospheric forcing used to drive both models includes three-hourly fields of sea-level atmospheric pressure and surface wind fields extracted from the North American Regional Reanalysis dataset (NARR; Mesinger *et al.*, 2006). The surface wind speed is converted to wind stress using the bulk formula of Large and Pond (1981). Hourly tidal forcing for eight major tidal constituents (M_2 , S_2 , N_2 , K_2 , O_1 , P_1 and O_1), in the form of tidal elevations and tidal currents specified at the lateral open boundaries of inner model, are produced by a tidal prediction system known as OTIS (Egbert and Erofeeva, 2002). In addition, the hourly wind-driven surface elevations and depth-averaged currents produced by the outer model are added to the open boundary conditions of the inner model (one-way nesting).

The surface heat flux for the inner model is calculated based on the model-calculated surface temperature in combination with three-hourly NARR fields of air temperature, cloud cover, downward shortwave radiation flux, and precipitation (Mellor, 2004). The subgrid scale horizontal mixing is calculated using the shear and grid size dependent scheme of Smagorinsky (1963). The vertical mixing is parameterized using the Mellor and Yamada (1982) level-2.5 turbulent closure scheme. To reduce model bias and drift from the observed seasonal cycle of hydrography, the spectral nudging technique

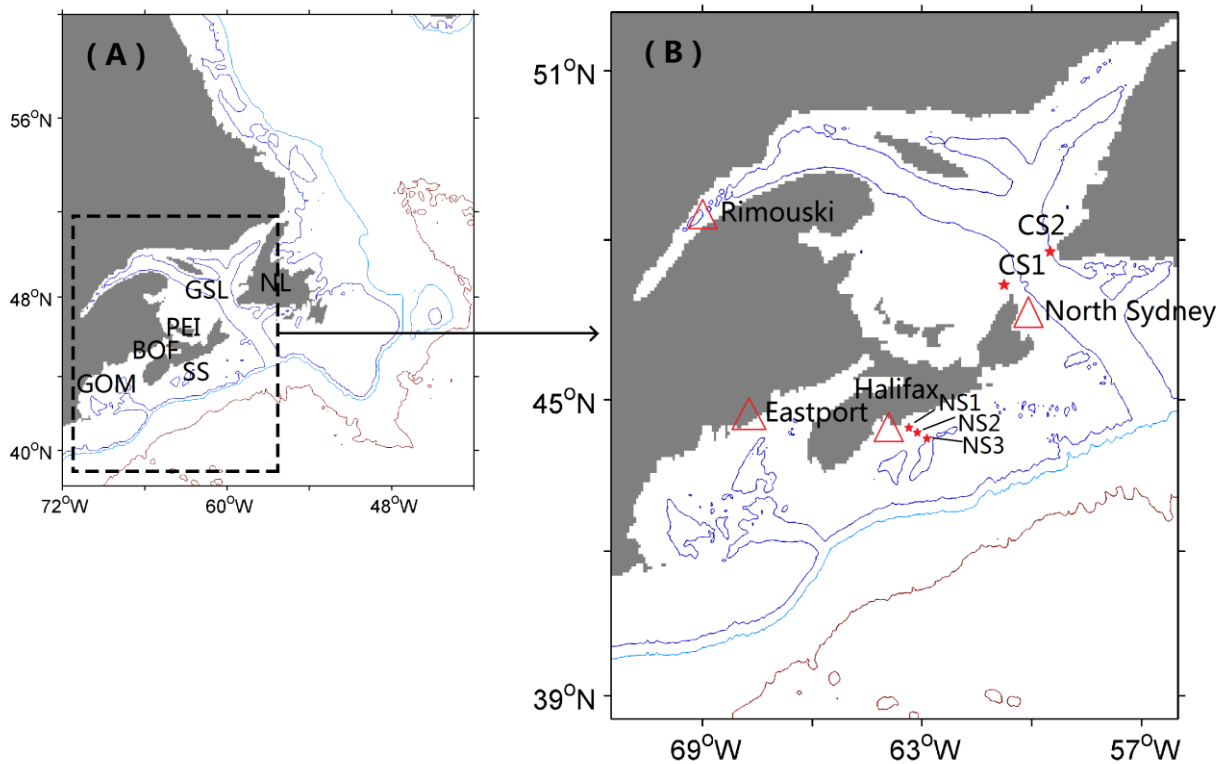


Figure 1. The domain and bathymetry of (A) the coarse-resolution outer model and (B) fine-resolution inner model of DalCoast. The 200, 1000, and 4000 meter depth contours of the model bathymetry are shown. Abbreviations are used for the Gulf of Maine (GoM), the Bay of Fundy (BoF), the Scotian Shelf (SS), Prince Edward Island (PEI), the Gulf of St. Lawrence (GSL), and Newfoundland (NL). The red triangles in (B) mark the positions of four tide gauges (Rimouski, North Sydney, Halifax, and Eastport). The red stars in (B) represent the approximate release locations for near-surface drifters along the Halifax line and drifters on Cabot Strait. In (B) three bottom-mounted ADCPs were located at the positions marked by red stars and labelled NS1, NS2 and NS3 over the central Scotian Shelf.

(Thompson *et al.*, 2007) and the semi-prognostic method (Sheng *et al.*, 2001) are applied in the inner model of DalCoast.

The nested-grid circulation modelling system is initialized from a state of rest with the model initial hydrography set to be the December mean hydrographic climatology. The modelling system is integrated for 25 months from the beginning of December 2006 to the end of December 2008. The model results in 2007 and 2008 are used for model validation and analysis.

2.2 Particle Tracking Model

Lagrangian trajectories of virtual particles (v-particles) carried passively or actively by ocean currents are very useful for estimating the fate of oil spills (Soomere *et al.*, 2010) or living organisms (Corell, 2012; Ohashi and Sheng, 2015), as well as for planning rescue operations or finding lost goods. In large enough quantities, Lagrangian trajectories of v-particles can be used to track entire water masses, or to map the mean flow (Richardson, 1983).

The particle tracking scheme used in this study is the one developed by Ohashi and Sheng (2015). The 3D movement of a v-particle carried by time-varying 3D ocean currents can be calculated as:

$$\vec{x}^{t+\Delta t} = \vec{x}^t + \int_t^{t+\Delta t} \vec{u}(\vec{x}, t) dt + \vec{\delta} \quad (1)$$

where $\vec{x}^{t+\Delta t}$ and \vec{x}^t are position vectors of a passive particle at time $t + \Delta t$ and previous time t respectively, $\vec{u}(\vec{x}, t)$ is the velocity vector of model currents, and $\vec{\delta}$ is the 3D random walk component to account for the subgrid scale turbulence and other local processes that are not resolved by the inner model. The 3D random walk component $\vec{\delta}(\delta x, \delta y, \delta z)$ in the x , y , and z directions can be expressed as (Taylor, 1922): $\delta x = \xi \sqrt{2K_h \Delta t}$, $\delta y = \xi \sqrt{2K_h \Delta t}$, $\delta z = \xi \sqrt{2K_z \Delta t}$. Here, ξ is a Gaussian random number in the range of $[-1, 1]$, K_h and K_z are the horizontal and vertical eddy diffusivity coefficients, and Δt is the time step (which is one hour in this study) used for time integration in Eq (1). Eddy

diffusivity coefficients (K_h and K_z) can vary in space and time. Past studies using drifters and numerical particle-tracking experiments (Tseng, 2002; Thompson *et al.*, 2002) suggested that the horizontal and vertical eddy diffusive coefficients in the coastal ocean vary from 0.1 to $10 \text{ m}^2 \text{ s}^{-1}$ and from 0.1×10^{-3} to $10 \times 10^{-3} \text{ m}^2 \text{ s}^{-1}$, respectively. In this study, the hourly inner model currents are used to driving this particle tracking scheme. We follow Shan and Sheng (2012), set the horizontal diffusivity coefficient for the random walk (K_h) to be $1.0 \text{ m}^2 \text{ s}^{-1}$, and set the vertical diffusivity (K_z) to be $1 \times 10^{-3} \text{ m}^2 \text{ s}^{-1}$. The fourth-order Runge-Kutta scheme (Press *et al.*, 1992) is used to track the passive particles.

3. Model Validation

DalCoast was validated extensively using various oceanographic observations in the past (Thompson *et al.*, 2007; Ohashi *et al.*, 2009a,b; Ohashi and Sheng, 2013, 2015). In this study, the performances of the inner model of DalCoast and the particle tracking model are further validated using three types of oceanographic observations. The first type of observations is the sea level observations at four tide gauge sites: (a) Rimouski on the northwestern GSL, (b) North Sydney on western Cabot Strait, (c) Halifax on the central Scotian Shelf, and (d) Eastport on the inner GoM. The tide gauge data were taken from the website of Department of Fisheries and Oceans, Canada. The locations of these four sites are shown in Figure 1B. The second type is the sub-surface current measurements made by three Acoustic Doppler Current Profilers (ADCPs) moored at locations NS1, NS2, and NS3 along the Halifax Line over the Scotian Shelf (Figure 1B, Baaren and Tang, 2009).

The third type of oceanographic measurements is the observed trajectories of near-surface drifters collected during the satellite-tracked surface drifter program by Baaren and Tang (2009). As part of this drift program, two drifter experiments were conducted respectively in October 2007 and October 2008. In October 2007, seven near-surface drifters were deployed at the 5-m depth along the Halifax line at three different sites (NS1, NS2, and NS3) during the fall cruise of Fisheries and Oceans Canada's Atlantic Zone Monitoring Program (AZMP) (Figure 1B). In October 2008, four near-surface drifters were deployed at 5 m over western Cabot Strait (CS1) and eastern Cabot Strait (CS2) respectively (Figure 1B). Two types of near-surface drifters were used respectively in the two drifter experiments. The first type of the drifters (Type 1), which was used for the first drifter experiment along the Halifax Line in October 2007, is the Self-Locating Datum Marker Buoy (SLDMB) manufactured

by Seimac. The Seimac drifter has a pyramid-shaped float above the water line, with an electronic unit underneath and a fishnet-type surface drogue tethered to the electronic unit. The second type of drifters (Type 2), which was deployed over Cabot Strait in October 2008 in the second drifter experiment, is also the SLDMB but manufactured by MetOcean Data Systems. The MetOcean drifter has a cylindrical hull for the electronics and four vanes with a foam float attached to it and an antenna above the hull. Position information of these drifters, including longitude, latitude and time, was collected half-hourly for the Seimac drifters and hourly for the MetOcean drifters. The data of the position information are transmitted to Argos satellites. Similar types of drifters were used to track ice drift previously by Baaren and Prinsenbergh (2000 a, b, 2001, 2006).

To quantify the model performance, we use the γ^2 index suggested by Thompson and Sheng (1997):

$$\gamma^2 = \frac{\text{Var}(O-M)}{\text{Var}(O)} \quad (2)$$

where Var represents the variance operator, and O and M denote the observed and model simulated variables respectively. Physically, the γ^2 index represents the ratio between the variance of the model hindcast errors and the variance of the observations. The smaller γ^2 is, the better is the model performance. In the case of the γ^2 index exceeding unity, the variance of the observation increases with the subtraction of the model results from the observations. In this study, $\gamma^2 = 1$ is chosen as a threshold value to assess the model performance.

3.2 Surface Elevations

Figure 2 presents time series of the observed and simulated surface elevations at four tidal gauge sites (Rimouski, North Sydney, Halifax and Eastport) during a 11-day period (1–12 October 2007). During this period, normal weather without any severe storms prevailed over the study region. Therefore, temporal variability of the surface elevations shown in Figure 2 is mostly associated with tidal elevations. The γ^2 values are about 0.089 at Rimouski, 0.105 at North Sydney, 0.057 at Halifax, and 0.035 at Eastport (Figure 3). These small γ^2 values indicate that about 89–96% of the total variance of the observed surface elevations at these four sites are accounted for by the model results. These small γ^2 values also indicate that the inner model of DalCoast has satisfactory hindcast skill in reconstructing the time evolution of surface elevations at these four sites.

To assess the model skill in simulating individual tidal constituents in the study region, a tidal harmonic analysis

was conducted to estimate amplitudes and phases of four major tidal constituents (M_2 , S_2 , K_1 and O_1) from time series of observed and simulated surface elevations at the four sites for October 2007. As shown in Table 1, the M_2 constituent estimated from observations at the four sites has amplitudes ranging from ~37 cm at North Sydney on Cabot Strait to ~261 cm at Eastport on the inner GoM. The S_2 constituent at the four sites has amplitudes ranging from ~8 cm at North Sydney to ~50 cm at Rimouski in the northwest GSL. By comparison, the K_1 constituent has relatively small amplitudes of about 7–17 cm at all four sites. The O_1 constituent has also relatively small amplitudes of about 5.1–10.6 cm at all four sites.

Table 1 also demonstrates that the inner model of DalCoast reproduces reasonably well the observed amplitudes and phases of M_2 at the four sites, with the

absolute model errors (differences between observations and model results) of about 2.3–9.5 cm in amplitude and between -8.4° and 6.4° in phase at the four sites. For S_2 , the model errors are about 0.6–2.2 cm in amplitude and between -3° and 2.8° in phase. The absolute model errors in amplitude and phase for these two major semidiurnal tidal constituents are generally small. For K_1 , the model errors are between -2.1 and 2.7 cm in amplitude and between -13° and 17° in phase. It should be noted that the relative model errors in amplitude are small and about 3–9% for the two major semi-diurnal tides (M_2 and S_2), but relatively large and about 6%–30% for the two diurnal tides (K_1 and O_1). Further studies are needed to examine the main physical processes affecting the performance of DalCoast in simulating these two diurnal tides.

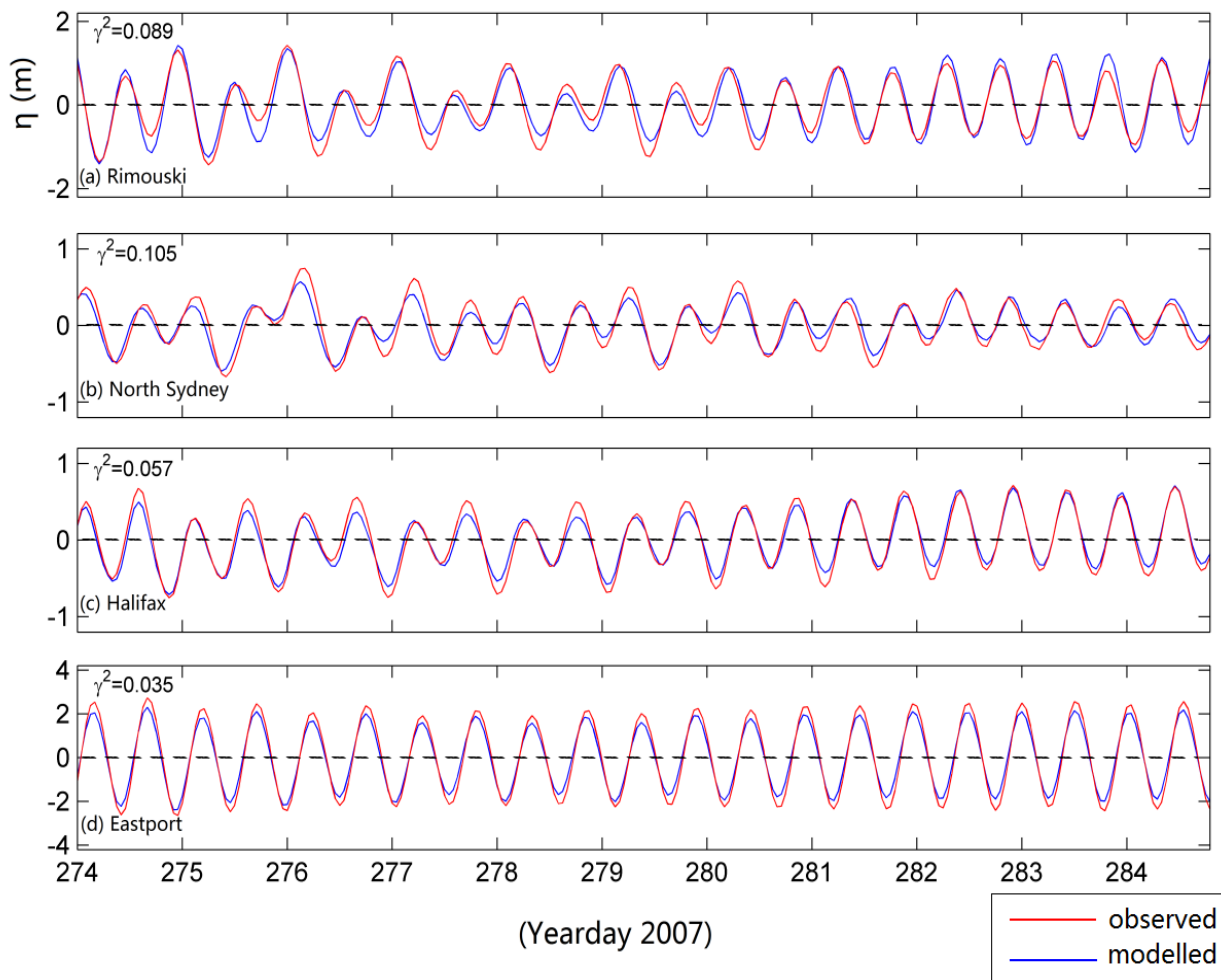


Figure 2. Time series of observed and simulated sea surface elevations at four sites of (A) Rimouski, (B) North Sydney, (C) Halifax, and (D) Eastport. These four sites are marked in Figure 1B. The simulated sea surface elevations are produced by the inner model of DalCoast.

Table 1. Amplitudes and phases of four major tidal constituents calculated from observed and simulated sea surface elevations in October 2007 at Rimouski, North Sydney, Halifax and Eastport.

Station	Amplitude (cm)			Phase (°)		
	Observed	Modeled	ΔH	Observed	Modeled	$\Delta\phi$
M_2						
Rimouski	131.52	123.81	7.71	347.17	345.93	1.24
North Sydney	37.33	35.04	2.29	104.86	98.50	6.36
Halifax	64.28	58.46	5.52	80.04	78.91	1.07
Eastport	261.44	252.19	9.25	131.83	140.23	-8.4
S_2						
Rimouski	49.67	48.06	1.61	300.77	300.18	0.59
North Sydney	8.25	7.70	0.55	251.57	251.99	-0.42
Halifax	15.89	14.79	1.10	22.87	20.06	2.81
Eastport	47.13	45.92	2.21	86.76	89.75	-2.99
K_1						
Rimouski	16.69	18.21	-1.52	296.92	284.41	12.51
North Sydney	10.81	9.67	1.14	347.20	330.37	16.83
Halifax	6.87	8.96	-2.09	124.45	140.25	-15.80
Eastport	10.74	8.08	2.65	195.82	188.61	-12.79
O_1						
Rimouski	27.92	29.70	-1.79	318.06	321.74	-3.68
North Sydney	8.19	10.60	-2.41	341.76	353.80	-12.04
Halifax	5.11	6.13	-1.02	170.68	185.63	-14.95
Eastport	11.97	8.43	3.33	329.32	306.45	22.87

We follow Pugh (2004) and quantify the type of tides at these four sites based on estimations of tidal amplitudes in Table 1 using the form factor (F) defined as

$$F = \frac{H_{O_1} + H_{K_1}}{H_{M_2} + H_{S_2}} \quad (3)$$

where H_{O_1} , H_{K_1} , H_{M_2} and H_{S_2} are respectively the amplitudes of diurnal tides K_1 and O_1 and semi-diurnal tides M_2 and S_2 based on observed or simulated values listed in Table 1. The tides are considered to be (a) semidiurnal for F values less than 0.25; (b) mixed and mainly semidiurnal for F values of 0.25–1.5, (c) mixed for F values of 1.5–3.0, and (d) mainly diurnal for $F > 3$. The form factor at Rimouski and North Sydney is about 0.25 and 0.42 respectively, indicating that the tides at these two sites are mixed and mainly semidiurnal (Figures 2A and 2B). The tides at Rimouski are more semidiurnal than those at North Sydney. The form factor is about 0.15 at Halifax and 0.07 at Eastport, indicating that tides at these sites are mainly semidiurnal (Figures 2C and 2D). The tides at Eastport are more purely semidiurnal than those at Halifax.

3.3 Sub-surface Currents

Figure 3 presents time series of observed and simulated currents at NS1, NS2, and NS3 for the 11-day period of 1–12 October 2007. These three sites were located inside

the main pathway of the Nova Scotia Current (Dever *et al.*, 2016). The Nova Scotia Current is a coastal current flowing southwestward over the inner Scotian Shelf (Petrie, 1987). This Current originates from the northwestern GSL, where a large-scale estuarine plume and an intense coastal jet known as the Gaspé Current are developed due to a large amount of freshwater discharge from the St. Lawrence River (El-Sabh, 1976; Tang, 1080; Sheng, 2001). The Gaspé Current spreads over the southwestern GSL and exits through western Cabot Strait. After emanating from western Cabot Strait, the low-salinity waters flow onto the eastern Scotian Shelf (ESS) to form the Nova Scotia Current (Petrie, 1987; Urrego-Blanco and Sheng, 2012).

The observed sub-surface currents shown in Figures 3A, 3B, 3G and 3H demonstrate that both the eastward and northward components of observed sub-surface currents at 15 m and 30 m at site NS1 have time-mean values of about -0.2 m/s during this 11-day period. These time-mean sub-surface currents represent the southwestward Nova Scotia Current. The observed sub-surface currents at site NS1 also have tidal currents and large synoptic (*i.e.*, mainly wind-driven) variabilities and significant sub-synoptic and seasonal variabilities. Tidal analysis indicates that the barotropic tides (not shown) account for small portions of observed temporal

variabilities at these two depths at NS1. At sites NS2 and NS3, by comparison, the observed sub-surface currents at 15 m and 30 m (Figures 3C, 3D, 3I and 3J) have similar temporal variabilities as those at site NS1, but with much weaker time-mean sub-surface currents at these two sites than at site NS1. Furthermore, the barotropic tidal currents (not shown) account for relatively large portions of the observed temporal variabilities of sub-surface currents at NS2 and NS3. It should be noted that the core

of the Nova Scotia Current was located near site NS2 (see Figure 6 of Dever *et al.*, 2016) in the period 2011–2014. The sub-surface current observations shown in Figure 3, however, indicate that the core of the Nova Scotia Current was located near site NS1 during the 11-day period in October 2007. Further studies are needed to explain the main physical processes affecting the onshore shift of this Current in October 2007.

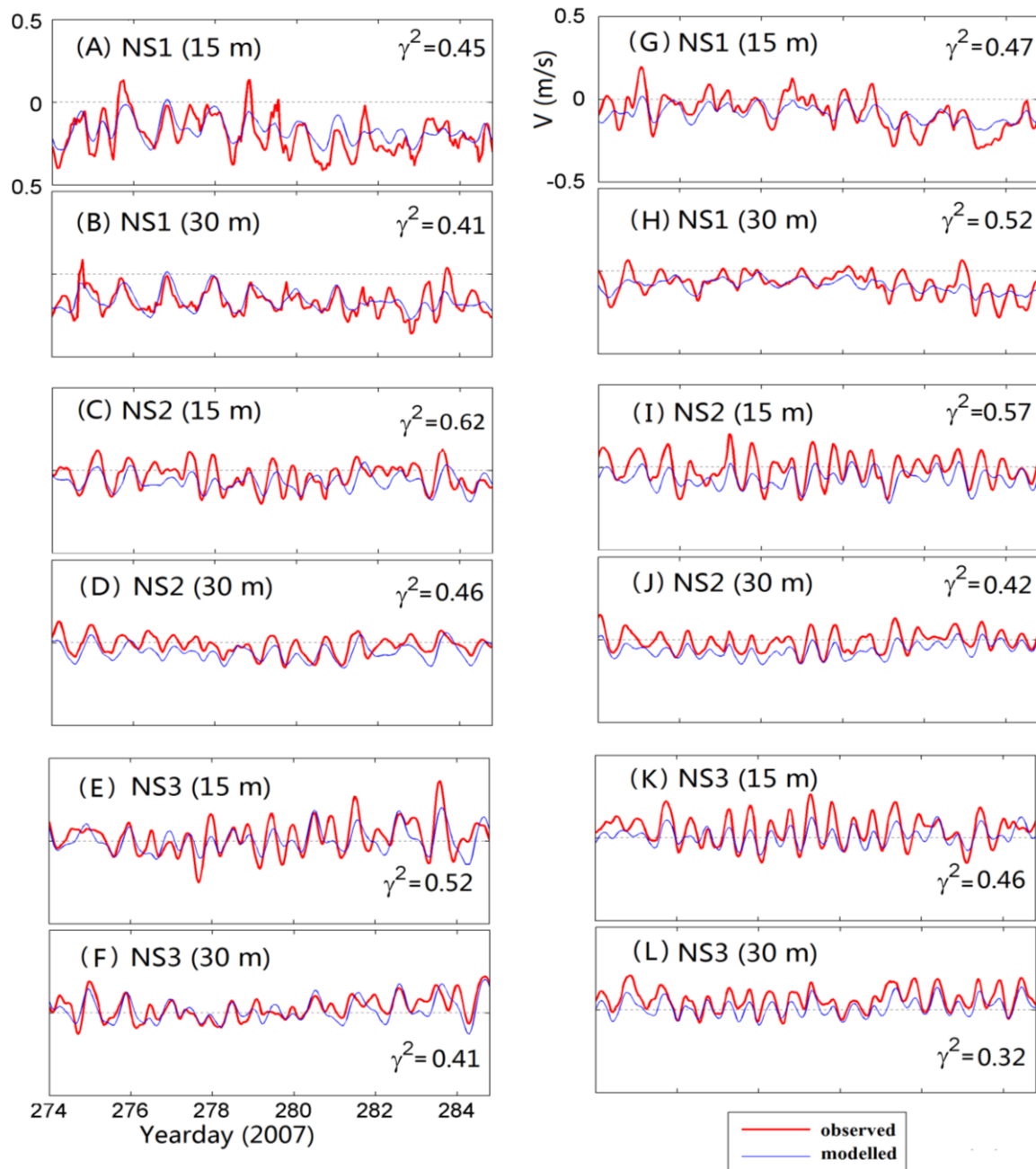


Figure 3. Time series of eastward (left) and northward (right) components of observed (red) and simulated (blue) sub-surface currents during a 11-day period in October 2007 at depths of 15 m and 30 m respectively at sites NS1, NS2, and NS3 along the Halifax Line over the central Scotian Shelf.

Figure 3 also demonstrates that the simulated sub-surface currents produced by the inner model of DalCoast agree reasonably well with the current observations at depths of 15 m and 30 m of these three sites. The γ^2 values are about 0.41–0.45 (0.47–0.52) for the eastward (northward) components of simulated currents at site NS1, 0.46–0.62 (0.42–0.57) for the eastward (northward) component at site NS2, and about 0.41–0.52 (0.32–0.46) for the eastward (northward) components at sites NS3. In comparison with the γ^2 values for the simulated surface elevations, the inner model of DalCoast reproduces less well the observed currents than the observed sea surface elevations. This could be explained by that fact that the ocean currents are more sensitive to the small-scale topography than sea surface elevations.

3.4 Particle Trajectories

To compare simulated trajectories calculated from model currents with observed trajectories of near-surface drifters, we conducted particle tracking experiments by releasing nearly 200 v -particles uniformly over a circular area of 4.4 km² centered around the release location of each SLDMB drifter. The main reason for releasing the v -particles over a small area instead of at a specific point is that actual movements of drifters are affected by many physical processes, including some small-scale processes that are not resolved in the circulation model.

In this section, we assess the performance of the particle tracking model by comparing the observed trajectory of a near-surface SLDMB drifter with the simulated trajectory of the horizontal “center of mass (CoM)” for a group of v -particles. The v -particles are released in an area surrounding the initial position of the real drifter. In this study, v -particles are set to remain in the surface waters. The hourly simulated currents produced by the inner model are used to drive the particle tracking model.

Since a small part of each SLDMB drifter was above the sea surface (Baaren and Tang, 2009), the observed trajectory of the real drifter was affected by winds at the sea surface. To account for the effect of winds on the observed trajectory, the velocity vector $\vec{u}(\vec{x}, t)$ in Eq. (1) is replaced by

$$\vec{u}(\vec{x}, t) = (1 - \alpha) \times \vec{u}_o(\vec{x}, t) + \alpha \vec{u}_w(\vec{x}, t) \quad (4)$$

where $\vec{u}_o(\vec{x}, t)$ is the ocean velocity vector produced by the inner model, $\vec{u}_w(\vec{x}, t)$ is the wind velocity vector, and α is the wind transfer coefficient, which is dependent of the volume and shape of the SLDMB drifter exposed to the wind at the sea surface. The wind’s effect on the drifter’s movement is also known as the leeway factor and has been a subject of past studies. For example,

Smith (1992) described a set of experiments using AST (Accurate Surface Tracker) in which a wind coefficient was parameterized in terms of the ratio of exposed to submerged frontal areas.

Figure 4 presents observed trajectories of type 1 SLDMB drifters (red solid lines) released at points very close to the ADCP sites NS1, NS2 and NS3 along the Halifax Line over the central Scotian Shelf (CSS). The four drifters were released between 11 October and 16 October 2007. For the two near-surface drifters released at points close to NS1, their trajectories over approximately five days after the release (Figures 4A and 4B) demonstrate that these drifters moved southwestward along the coastline with average speeds of about 30 km/day. The near-surface drifter released at the point close to site NS2 (Figure 4C) moved approximately westward first and then southwestward, roughly parallel to the coastline, for five days, with a lower average speed of about 15 km/day. The near-surface drifter released at the point close to site NS3 drifted near its release point (Figure 4D), moving northwestward, northeastward, then southeastward. The observed movements of the four near-surface drifters shown in Figure 4 are roughly consistent with the general circulation over the central Scotian Shelf indicated by the sub-surface current measurements shown in Figure 3.

The simulated (CoM) trajectories of v -particles with six different wind transfer coefficients (α) ranging between 0 and 0.03 (colored dashed lines) are also shown in Figure 4. The v -particles released over a small area close to NS1 (with $\alpha \leq 0.03$) (Figures 4A and 4B) have significant southwestward (alongshore) movements, which are very similar to the SLDMB drifters released at the same points. The v -particles released over a small area close to NS2 (Figure 4C) have moderate alongshore movements in comparison with those shown in Figures 4A and 4B. The v -particles released at a small area close to NS3 stay close to their release area (Figure 4D), with much smaller net displacements in comparison with those in Figures 4A and 4C. Some noticeable differences occur in simulated trajectories for different values of wind transfer coefficients (α), indicating the effects of surface winds on the movements of v -particles.

Figure 5 presents the observed trajectories for type 2 SLDMB drifters released at points close to sites CS1 and CS2 over western and eastern Cabot Strait, respectively. The two drifters are released between 16th October to 20th October 2008. The two SLDMB drifters released at points close to CS1 had significant southeastward movements during the first three days then turned southwestward to move onto the eastern Scotian Shelf on the last day (Figures 5A and 5B). By comparison, the SLDMB

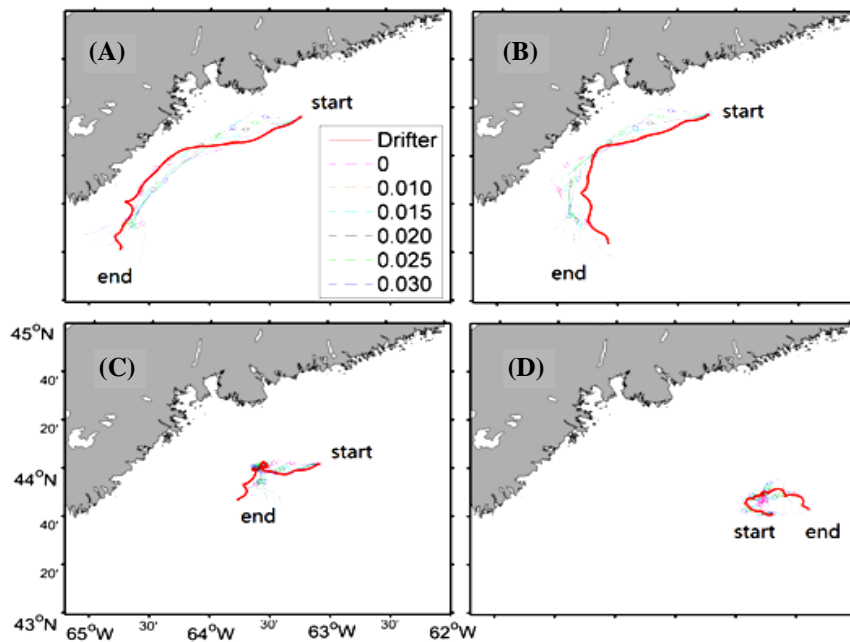


Figure 4. Comparisons of observed trajectories (red solid lines) with simulated CoM trajectories (coloured dashed lines) calculated by the particle tracking model with different wind transfer coefficients for v-particles released over a small area centered at (A) NS1, (B) NS1, (C) NS2 and (D) NS3 along the Halifax Line over the central Scotian Shelf. The circles mark positions at 24-hour intervals.

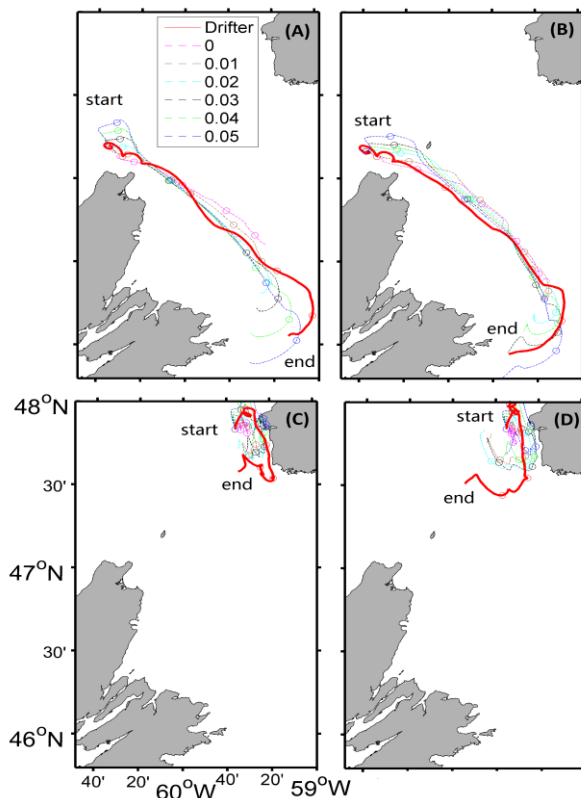


Figure 5. Comparisons of observed trajectories (red solid lines) with simulated CoM trajectories (coloured dashed lines) calculated by the particle tracking model with different wind transfer coefficients for v-particles released over a small area centered at (A) CS1, (B) CS1, (C) CS2 and (D) CS2 over Cabot Strait. The circles mark positions at 24-hour intervals.

drifters released at points close to CS2 moved northeastward during the first day (Figures 5C and 5D). They reversed directions to travel southward, parallel to the local coastline, for the next two days and then moved westward/northwestward during the last two days. Figure 5 also demonstrates that the v-particles released in small areas close CS1 and C2 (with $\alpha \leq 0.05$) have trajectories very similar to the observed trajectories of SLDMB drifters.

One important issue raised when comparing trajectories of real drifters with those of v-particles is the optimal value of the wind transfer coefficient for each type of drifters. To address this issue, we calculate the separation distance (Δr) between the SLDMB drifter and the CoM of v-particles over 120 hours following the release of the drifters/v-particles. Figure 6A presents time series of separation distances for the drifter experiment in October 2007 using type 1 SLDMB drifters with six different α values for the v-particles. The separation distances increase with time during the first 40 hours. After reaching maximum values at about 40 hours, the separation distances decrease with time and reach minimum values at about 80 hours and then increase with time after 100 hours. Figure 6C demonstrates the separation distances for the second drifter experiment in October 2008 using type 2 SLDMB drifters with six different α values for the v-particles. The separation distances for the second drifter experiment increase with time with significant perturbations during the 120 hours after the releases. It should be noted that the temporal variabilities of separation distances are affected by many processes, including ocean currents, surface wind speeds and wind

transfer coefficients.

Based on time series of separation distances shown in Figures 6A and 6C, we calculate the time mean separation distances averaged over 120 hours (mean error) and show them in Figures 6B and 6D as a function of α . The optimal value for the wind transfer coefficient is $\alpha \approx 0.015$ for type 1 SLDMB drifters and $\alpha \approx 0.030$ for type 2 SLDMB drifters.

4. Retention, Dispersion and Hydrodynamic Connectivity

Simulated trajectories of v-particles carried passively by ocean currents produced by the inner model of DalCoast (with $\alpha = 0$) are used to estimate the retention, dispersion and hydrodynamic connectivity over the Scotian Shelf and adjacent waters (including the southwestern GSL, inner GoM and BoF).

4.1 Retention and Dispersion Over the Eastern Canadian Shelf

To quantify retention and dispersion of passive particles, we follow Cong *et al.* (1996) and introduce the retention index. The study area is first divided into subareas of equal size. The retention index is then defined as:

$$R(\vec{x}, t) = \frac{N(\vec{x}, t)}{N(\vec{x}, t_0)} \quad (5)$$

where $N(\vec{x}, t_0)$ is the number of v-particles released initially in a subarea of a given size centered at \vec{x} at initial time t_0 , and $N(\vec{x}, t)$ is the number of v-particles remaining within the subarea at some later time t . Physically, the retention index represents the proportion of v-particles released in a giving subarea at time t_0 remaining at a later time t . The value of retention index $R(\vec{x}, t)$ is between 0 and 1. A high value of $R(\vec{x}, t)$ corresponds to high retention of v-particles in the given subarea. In the case of $R(\vec{x}, t) = 0$, all the v-particles released at time t_0 are flushed out from the subarea by time t . The subarea used in this study is set to a square box with a horizontal dimension of $33 \times 33 \text{ km}^2$. To eliminate the effect of small-scale circulation features from the experiment results, the distance between centers of two adjacent boxes is set to 3.5 km. To calculate the retention indices over the study region, the v-particles are released in a horizontally uniform pattern in the surface waters of top 5 m over the inner model domain. The initial horizontal distance between two adjacent v-particles is set to 2000 m (or ~ 270 v-particles per 1000 km^2). The retention indices are calculated based on movements of v-particles using the hourly surface currents produced by the inner model in February, May, August, and November 2007 (Figure 7).

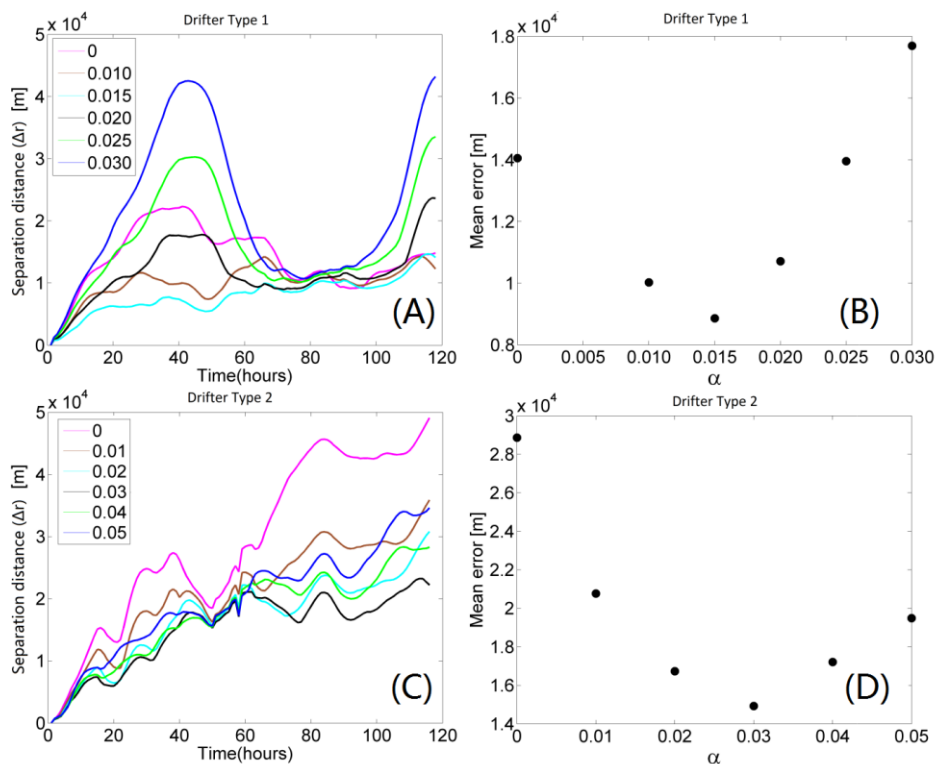


Figure 6. (A, C) Time series of separation distances (Δr) between real and simulated drifters in terms of different wind transfer coefficient values. (B, D) Separation distances averaged over the experiment period. Results are for (A) type 1 and (B) type 2 of SLDMB drifters.

The horizontal distributions of retention indices on day 5 (R_5) have similar large-scale features (Figure 7) in the four months, with relatively high retention indices (60–80%) over the BoF, inner GoM, central and ESS, Northumberland Strait, and Magdalen Shallows. Relatively low retention indices (30%–40%) occur over narrow coastal zones over western and eastern Cabot Strait, and the inner shelf and the shelf break of the Scotian Shelf. The low retention indices over these regions are consistent with relatively strong surface currents (see more discussion in section 4.2). The R_5 distributions also have significant seasonal variabilities. Over the middle and outer shelf regions of the ESS and central Scotian Shelf (CSS), the R_5 values are relatively high in February, August and November and relatively low in May. Over the Magdalen Shallows, the R_5 values are relatively high in February, May and August and relatively low in November. Over the inner GoM and

BoF, the R_5 values are relatively high in November and relatively low in May and August.

The large-scale features of retention indices on day 10 (R_{10}) are similar to those on day 5, except that regions with high retention indices (60%–80%) on day 10 are significantly reduced (Figure 7). In particular, the R_{10} values are low (less than 30%) in these four months over western Cabot Strait, inner Scotian Shelf, outer shelf regions of the western Scotian Shelf (WSS). Relatively large R_{10} values (70%) occur over Northumberland Strait in the four months, over the middle of the eastern Scotian Shelf in August and September, and over coastal waters off western Nova Scotia in February.

The retention indices on days 15 and 20 (R_{15} and R_{20}) are generally low over the study region, except for coastal waters around Northumberland Strait, some offshore areas of the SS, and coastal waters in the BoF (Figure 7).

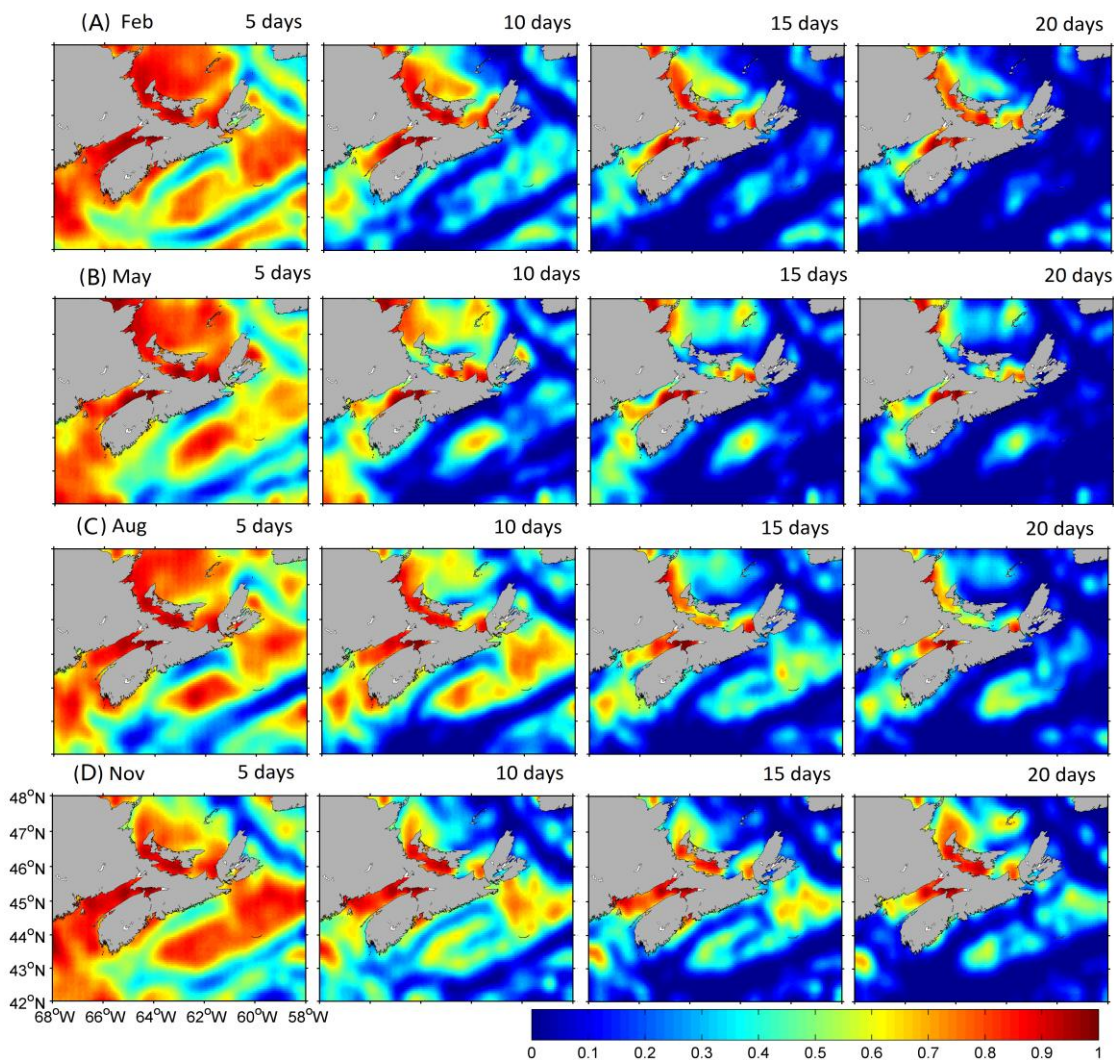


Figure 7. Distributions of retention indices over the Scotian Shelf and adjacent waters (including the southwestern GSL, inner GoM and BoF) calculated from horizontal movements of near-surface v -particles driven by hourly near-surface current produced by the inner model in (A) February, (B) May, (C) August, and (D) November 2007.

4.2 Physical Processes Affecting Retention and Dispersion

As shown in the previous section, the horizontal distributions of retention (or dispersion) calculated from simulated trajectories of near-surface v-particles have significant temporal and spatial variability. To quantify the main physical processes affecting the retention and dispersion over the Scotian Shelf and adjacent waters, three different numerical experiments were conducted. The model setups and the sub-grid scale mixing parameterizations are the same but the model's external forcings are changed among the experiments as follows:

1. Control Run (CR): The circulation modelling system (DalCoast) in this experiment is driven by all forcing terms as discussed in section 2, which include tidal forcing, wind forcing, atmospheric pressures, sea surface heat fluxes, river runoff and open boundary forcing.
2. No Tides (NT): Same as the CR, except that the tidal forcing is excluded from this experiment. Specifically, both the tidal currents and tidal elevations are set to zero along the open boundaries of the inner model.
3. No Wind (NW): Same as the CR, except that the local wind stress is set to zero in the inner model.

The model results from these three experiments are then used to quantify the role of the tides and local wind over the SS and adjacent waters. Let $\varphi_{CR}, \varphi_{NT}, \varphi_{NW}$ be the model results from the model run CR, NT and NW, respectively. The effects of the tidal forcing can be estimated by

$$\Delta\varphi_{tide} = \varphi_{CR} - \varphi_{NT} \quad (6)$$

Similarly, the effects of the local wind forcing can be quantified approximately by

$$\Delta\varphi_{wind} = \varphi_{CR} - \varphi_{NW} \quad (7)$$

Figure 8 presents the effect of tidal forcing ($\Delta\varphi_{tide}$) on retention indices over the Scotian Shelf and adjacent waters on day 20 in the four months of February, May, August, and November 2007. The common feature of the tidal effects in these four months is that the tidal forcing reduces the retention indices in the BoF by about 40%–50%. This means the tidal flow facilitates the dispersion of near-surface waters in the BoF. The tidal forcing also reduces the retention indices over coastal waters off southwest Nova Scotia in May, August, and November, but enhances the retention indices over the same coastal waters in February.

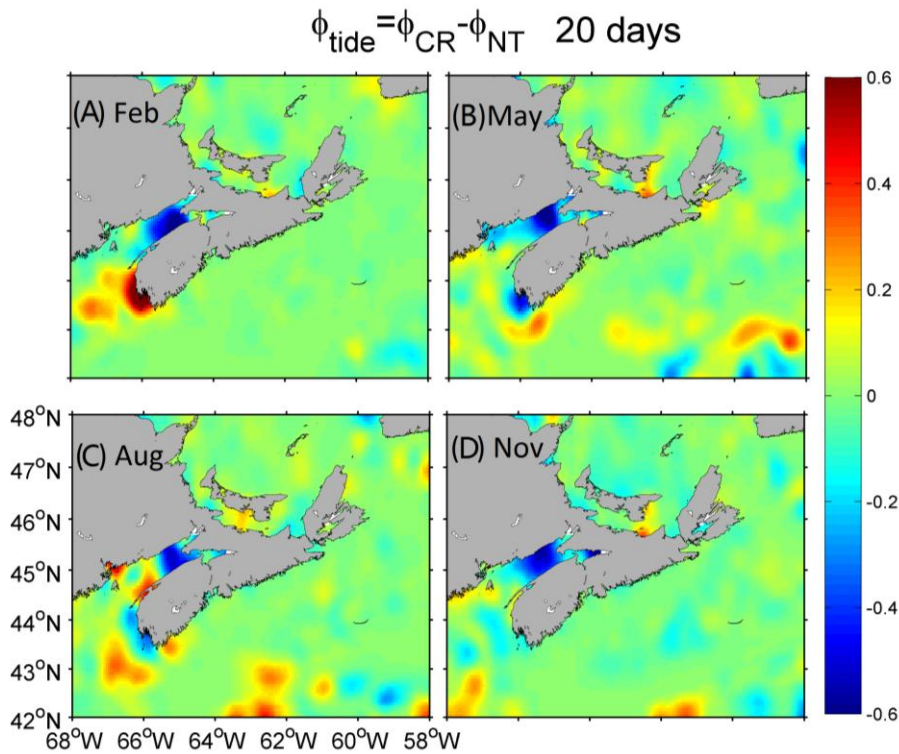


Figure 8. Distributions of retention indices due to the tidal forcing ($\Delta\varphi_{tide}$) on 20 days over the Scotian shelf and adjacent waters in (A) February, (B) May, (C) August, and (D) November 2007.

Figure 9 presents the effect of local wind forcing ($\Delta\phi_{wind}$) on retention indices over the Scotian shelf and adjacent waters on day 20 in the four months of February, May, August, and November. The wind forcing reduces the retention indices over the southwestern GSL and western Cabot Strait in the four months (with the most significant reduction in February when the local winds are strongest), and also reduces the retention indices over the ESS in February and May. However the wind forcing enhances the retention over coastal waters off the southwest Nova Scotia in February, May, and August and enhances the retention over the ESS in November.

It should be noted that the wind forcing over the study region exhibits strong seasonal variability (Figure 10). In February and May of 2007, winds are roughly eastward. In August, winds blow from the southwest and are weaker than in other seasons. In November, winds are roughly southward in the GoM and northeastward over the Scotian Shelf and the GSL. The large seasonal variability in the local wind forcing introduces large seasonal variability in the surface circulation over the study region, leading to large seasonal variabilities in the retention indices as shown in Figure 9.

The local wind forcing enhances the surface currents over the Magdalen Shallows in all four months (Figure 10). In consequence, the transportation of the near-surface

particles from GSL to SS is facilitated. In February, the eastward winds generate southeastward offshore currents over the outer shelf region of the Scotian Shelf (Figures 10A-1 and 10A-2). This offshore current disperses the near-surface particles, which is consistent with the coastline retention reduction (Figure 9A). In August and November, the northeastward winds decelerate the Nova Scotian current and even generate reverse flows along parts of the coastline (Figures 10C and 10D), which is consistent with the coastline retention addition (Figures 9C and 9D). In February, May, and August, the eastward winds generate onshore surface current and enhance the retention indices along the western coastline of Nova Scotia. However in November, the southward winds do not have significant effects along the same location.

4.3 Hydrodynamic Connectivity

In this section, we examine the hydrodynamic connectivity for three sensitive areas in the study region in terms of upstream and downstream areas using the simulated trajectories of near-surface v-particles. The upstream (or source) area of a given site (or area) is defined as the area from which particles (or material) are transported to the site. The downstream (or sink) area of a given site (or area) is defined as the area to which particles are transported from the site.

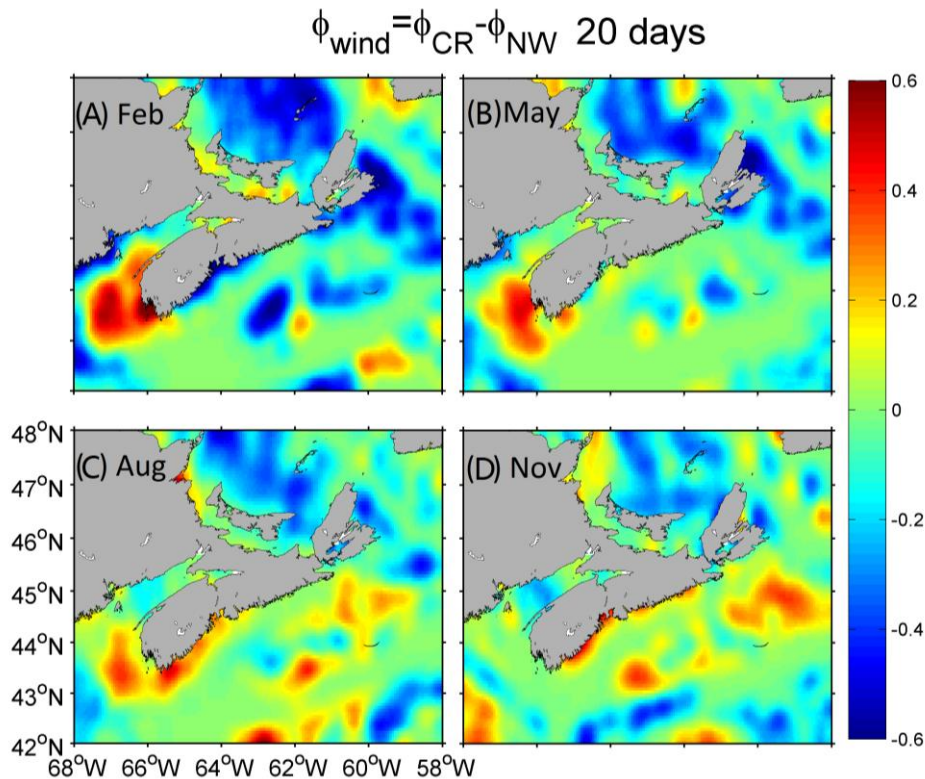


Figure 9. Distributions of retention indices due to wind forcing ($\Delta\phi_{wind}$) on 20 days over the Scotian Shelf and adjacent waters in (A) February, (B) May, (C) August, and (D) November 2007.

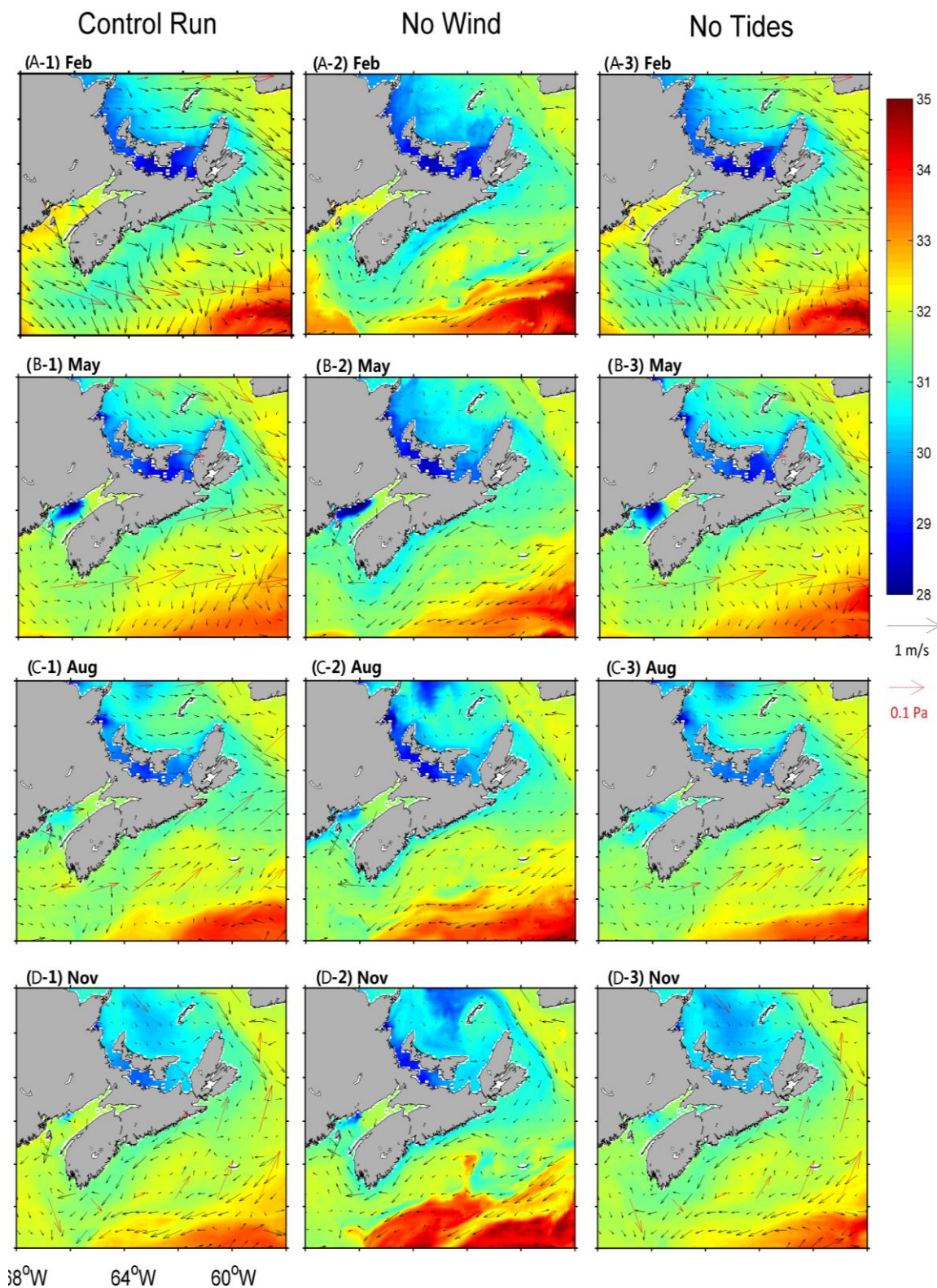


Figure 10. Mean surface currents and salinity fields (Control Run, No Wind and No tides) produced by inner model for 20 days in (A) February, (B) May, (C) August, and (D) November in 2007. Red arrows are wind stress vectors. For clarity, velocity vectors are plotted at every seventh model grid point.

The three areas selected for this study are (a) St. Anns Bank, (b) Deep Panuke offshore oil and gas platforms, and (b) the outer Bay of Fundy. St. Anns Bank has been selected by the Fisheries and Oceans Canada as a new area of interest for potential designation as a Marine Protected Area (Ford and Serdyska, 2013). The Bay of Fundy is known for its high tides with a maximum tidal range of about 16.9 m. A demonstration project for harnessing tidal energy using “In-stream turbine technology” has been conducted in the eastern part of the BoF (Lambert, 2016).

We follow Tang *et al.* (2006) and define the downstream area as the sum of all subareas to which more than 2% of particles originally released over the surface of a given source area travel within 20 days. Similarly, the upstream area of a designated sink area is defined as the sum of all subareas from which at least 2% of particles in the sink area originated during the previous 20 days. Physically, the downstream area defined here is a potential area to which the surface particles could be exported from the designated source area within a given time as 20 days. The upstream area is a potential area from which the passive particles could be transported to a

designated sink area within the same period. The size of the subareas used in this section is the same as that used in the calculation of retention indices discussed in section 4.1.

The 20-day downstream (sink) area for the St. Anns Bank (DA_{SAB}) consists of the main part over the inner shelf of the ESS and a small part along the eastern flank of the ESS (Figure 11). The former is associated with the main pathway of the southwestward Nova Scotia Current over the coastal waters of the ESS. The latter is associated with a small branch of the outflow emanating from the GSL that continues to flow southeastward along the eastern flank of the ESS. The pattern of DA_{SAB} has large seasonal variabilities. The main part of (DA_{SAB}) over the inner shelf of the ESS extends most significantly southwestward (alongshore) to reach coastal waters off Taylor Head in February (Figure 11A) and spreads offshore most significantly to the middle of the ESS in November (Figure 11D). A small part of (DA_{SAB}) reaches the shelf waters to the south of Misaine Bank and Eastern Shoal in February and May (Figures 11A and 11B) and reaches the shelf break waters to the southern Banquereau Bank over the ESS in November.

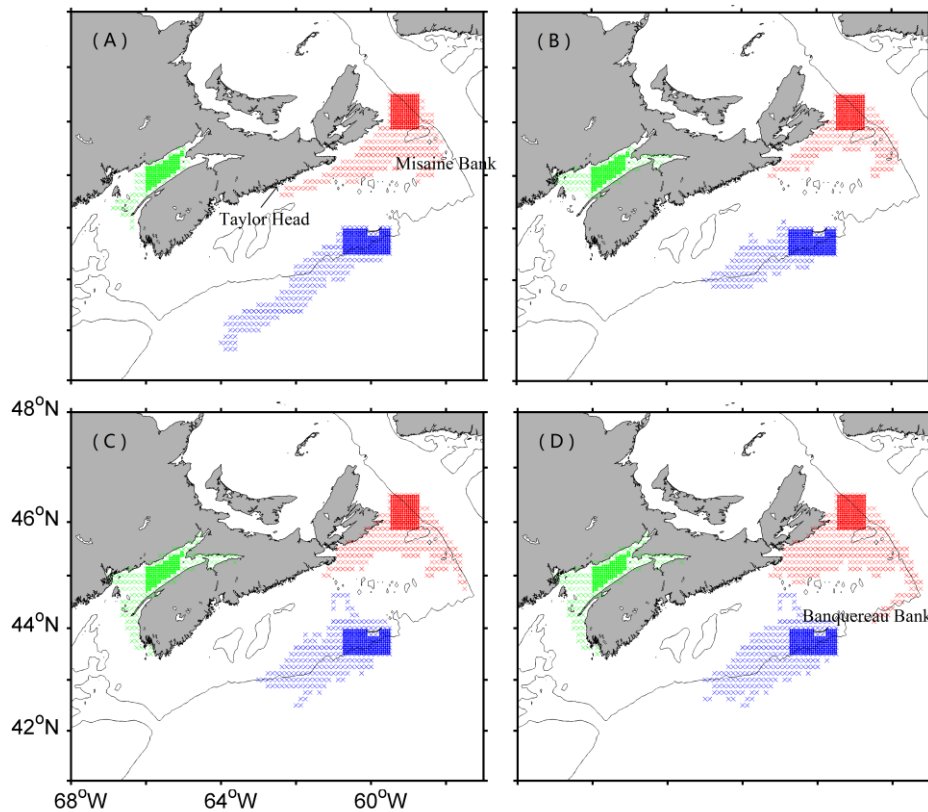


Figure 11. Downstream (sink) areas for (A) St. Anns Bank (red), (B) the Deep Panuke Offshore Platforms (blue), and (C) the outer Bay of Fundy (green) within 20 days calculated from the hourly current field produced by the inner model in (A) February, (B) May, (C) August, and (D) November 2007. The 200-m water depth contours are shown as black lines.

The 20-day downstream area for the Deep Panuke offshore oil and gas platforms (DA_{DP}) cover a narrow corridor to the west/southwest of the platform as a result of the southwestward jet over the shelf break of the CSS. The narrow corridor is centered over the shelf break of the CSS in May, August, and November. In February, by comparison, the narrow corridor extends further southwestward to reach the northwest Atlantic Ocean waters off the shelf break of the western Scotian Shelf (WSS). The horizontal dimension of DA_{DP} is about 400 km by 100 km in February and 200 km by 200 km in other months. In August, the DA_{DP} also has a narrow stripe extending northward from the platforms to the inner shelf of the ESS.

The 20-day downstream area for the outer Bay of Fundy (DA_{BOF}) covers over the coastal waters outside the BoF and off the western Nova Scotia in the four months (Figure 11). In May, August and November, DA_{BOF} also includes the surface waters over the inner BoF. It should be noted that D_{BOF} is significantly smaller than DA_{SAB} and DA_{DP} .

Figure 12 presents the 20-day upstream (source) areas for the above three selected shelf areas in February, May,

August and November. The 20-day upstream area for St. Anns Bank (UA_{SAB}) covers surface waters over western Cabot Strait and adjacent southern GSL and centered over waters of about 200 m depth in the four months, associated with the southeastward flow from the GSL to the ESS. The upstream area UA_{SAB} extends significantly northward to the central GSL in February and November in comparison with those in May and August (Figures 12B and 12C). The upstream area UA_{SAB} is largest in November (Figure 12D) and smallest in August among the four months. Furthermore, the source area for St. Anns Bank also includes surface waters over the western Grand Banks in February and November (Figures 12A, and 12D), associated with a cross-channel flow from the western Grand Banks to the ESS in these two months.

The 20-day upstream area for the Deep Panuke offshore oil and gas platforms (UA_{DP}) is a narrow zone centered around the 200-m water depth over the shelf break to the east of the platforms in the four months and some surface waters over the western side of the mouth of the Laurentian Channel (Figure 12). The pattern of UA_{DP} is consistent with the southwestward jet over the shelf break of the ESS.

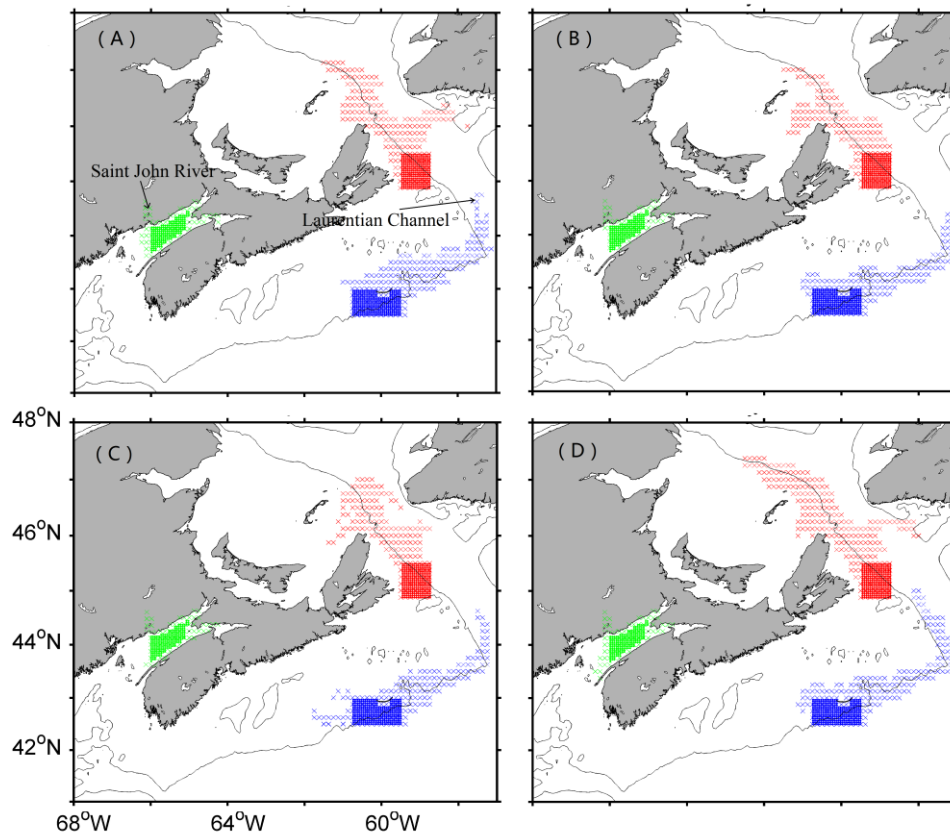


Figure 12. Upstream (source) areas for (A) St. Anns Bank (red), (B) the Deep Panuke Offshore Platforms (blue), and (C) the outer Bay of Fundy (green) within 20 days calculated from the hourly current field produced by the inner model in (A) February, (B) May, (C) August, and (D) November 2007. The 200-m water depth contours are shown as black lines.

The 20-day upstream area for the outer Bay of Fundy (UA_{BoF}) includes surface waters over the inner BoF and the Saint John River, with some surface waters outside the BoF (Figure 12). In comparison with St. Anns Bank and Deep Panuke platforms, the outer Bay of Fundy has a much smaller source region, is limited mainly to the inner BoF.

5. Summary and Conclusions

A nested-grid circulation modelling system and a Lagrangian particle tracking model were used to study the three-dimensional circulation, particle movements, retention, dispersion and connectivity over the Scotian Shelf, southern Gulf of St. Lawrence (GSL), inner Gulf of Maine (GoM), Bay of Fundy (BoF) and their adjacent deep ocean waters. The circulation modelling system has a fine-resolution baroclinic inner model nested inside the coarse-resolution barotropic outer model. A conventional one-way nesting technique was used to transfer information from the outer model to the inner model. The model validation presented in this study and in previous studies made by Thompson *et al.*, (2007), and Ohashi *et al.*, (2009a, b) and Ohashi and Sheng (2013) demonstrated that the inner model has reasonable skills in simulating sea surface elevations, ocean currents and hydrography over the study region. Hourly model currents produced by the inner model were used to track movements of near-surface virtual particles (v-particles) over the study region.

Retention indices (R) for surface waters over the study region were calculated based on the simulated movements of v-particles carried passively by surface ocean currents. The horizontal dispersion rate can be calculated from $(1-R)$. It was found that the retention within 10 days is relatively high for surface waters in Northumberland Strait, over the outer shelves of the eastern and central Scotian Shelf (ESS and CSS), in the outer and central BoF, and over the inner GoM. By comparison, the retention is relatively low for surface waters over western Cabot Strait and the part of southern GSL adjacent to it, over the inner shelf of the ESS and CSS, and outer shelf of the western Scotian Shelf (WSS), and along the shelf break and its adjacent waters of the Scotian Shelf. The regions with low retention are associated with relatively strong and persistent surface currents.

The upstream (source) and downstream (sink) areas for surface waters over (a) St. Anns Bank, (b) Deep Panuke offshore oil and gas platforms and (c) the outer BoF were also calculated from simulated movements of near-surface v-particles. The main upstream area for surface waters over St. Anns Bank is a narrow corridor to the northeastward of the Bank, which covers offshore

surface waters centered around the 200-m water depth over western Cabot Strait and adjacent southern GSL. The downstream area for surface waters over St. Anns Bank covers mainly surface waters over the inner shelf of the ESS. For the Deep Panuke offshore oil and gas platforms, the upstream area is a narrow strip over the shelf break of the ESS, and the downstream area is the relatively broad strip of surface waters over the shelf break and adjacent deep ocean waters off the central Scotian Shelf. By comparison, the upstream area for the outer BoF is very small and limited mostly to surface waters over the inner Bay of Fundy and the Saint John River. The downstream area for the outer BoF includes coastal waters outside the BoF and off western Nova Scotia and also some surface waters over the inner BoF. It should be noted that the simulated movements of v-particles, retention indices, and upstream and downstream areas have significant seasonal variability. More studies are needed to examine the interannual and decadal variabilities of circulation, retention and hydrodynamic connectivity of surface and sub-surface waters over the Scotian Shelf and adjacent waters.

Acknowledgements

This study was supported by the Ocean Tracking Network (OTN), the Marine Environmental Observation Prediction and Response Network (MEOPAR), and the Ocean Frontier Institute (OFI), Lloyd's Register, and the academic research contribution program of Fisheries and Oceans Canada. JS was also supported by the Natural Sciences and Engineering Research Council of Canada (NSERC). MEOPAR is funded by the Government of Canada's Networks of Centers of Excellence Program. Comments from two reviewers led to improvements in the manuscript and are acknowledged.

References

- Cong L, Sheng J and Thompson K T. (2002). A retrospective study of particle retention on the outer banks of the Scotian Shelf 1956-1993. *Rheumatology*, 41(1): 10-108.
- Corell H. (2012). Applications of ocean transport modelling [Internet]. University of Stockholm. <http://www.diva-portal.org/smash/get/diva2:516366/FULLTEXT01.pdf>
- Dever M, Hebert D, Greenan B J W, *et al.* (2016). Hydrography and coastal circulation along the Halifax Line and the connections with the Gulf of St. Lawrence. *Atmosphere-Ocean*, 54(3): 199-217. <https://dx.doi.org/10.1080/07055900.2016.1189397>
- El-Sabh M I. (1976). Surface circulation pattern in the Gulf of St. Lawrence. *Journal of the Fisheries Research Board of Canada*, 33(1): 124-138.

- <https://dx.doi.org/10.1139/f76-015>
- Egbert G D and Erofeeva S Y. (2002). Efficient inverse modeling of barotropic ocean tides. *Journal of Atmosphere and Oceanic Technology*, 19(2): 183–204.
[https://dx.doi.org/10.1175/1520-0485\(2000\)030<0015:SA MFEO>2.0.CO;2](https://dx.doi.org/10.1175/1520-0485(2000)030<0015:SA MFEO>2.0.CO;2)
- Urho L. (1999). Relationship between dispersal of larvae and nursery areas in the Baltic Sea. *ICES Journal of Marine Science*, 56(6): 114–121.
<https://dx.doi.org/10.1006/jmsc.1999.0634>
- Large W and Pond S. (1981). Open ocean momentum flux measurements in moderate to strong winds. *Journal of Physical Oceanography*, 11(3): 324–336.
[https://dx.doi.org/10.1175/1520-0485\(1981\)011<0324:OOMFMI>2.0.CO;2](https://dx.doi.org/10.1175/1520-0485(1981)011<0324:OOMFMI>2.0.CO;2)
- Loder J W, Petrie B and Gawarkiewicz G. (1998). The coastal ocean off northeastern North America: A large scale view. In: Robinson AR, Brink KH (editors). *The sea, 11: The global coastal studies. Regional studies and syntheses*. New York: Wiley, 105–133.
- Mellor G L. (2004). Users guide for a three dimensional, primitive equation, numerical ocean model. *Program in Atmospheric and Oceanic Science*, Princeton Univ. Princeton, N. J.
- Mellor G L and Yamada T. (1982). Development of a turbulence closure model for geophysical fluid problems. *Reviews of Geophysics*, 20(4): 851.
<https://dx.doi.org/10.1029/rg020i004p00851>
- Mesinger F, DiMego G, Kalnay E, et al. (2006). North American Regional Reanalysis. *Bulletin of the American Meteorological Society*, 87: 343–360.
<https://dx.doi.org/10.1175/BAMS-87-3-343>
- Ohashi K, Sheng J, Thompson K, et al. (2009a). Effect of stratification on tidal circulation over the Scotian Shelf and Gulf of St. Lawrence: A numerical study using a three-dimensional shelf circulation model. *Ocean Dynamics*, 59(6): 809–825.
<https://dx.doi.org/10.1007/s10236-009-0212-7>
- Ohashi K, Sheng J, Thompson K, et al. (2009b). Numerical study of three-dimensional shelf circulation on the Scotian Shelf using a shelf circulation model. *Continental Shelf Research*, 29(17): 2138–2156.
<https://dx.doi.org/10.1016/j.csr.2009.08.005>
- Ohashi K and Sheng J. (2013). Influence of St. Lawrence River discharge on the circulation and hydrography in Canadian Atlantic waters. *Continental Shelf Research*, 58(5): 32–49.
<https://dx.doi.org/10.1016/j.csr.2013.03.005>
- Ohashi K and Sheng J. (2015). Investigating the effect of oceanographic conditions and swimming behaviours on the movement of particles in the Gulf of St. Lawrence using an individual-based numerical model. *Atmosphere -Ocean*, 54(3): 278–298.
<https://dx.doi.org/10.1080/07055900.2015.1090390>
- Petrie B. (1987). Undulations of the Nova Scotia current, *Atmosphere-Ocean*, 25(1): 1–9.
<https://dx.doi.org/10.1080/07055900.1987.9649260>
- Press W, Teukolsky S, Vetterling W, et al. (1992). *Numerical recipes in fortran: The art of scientific computing*. New York: Cambridge University Press.
- Richardson P L. (1983). Eddy kinetic energy in the North Atlantic from surface drifter. *Journal of Geophysical Research*, 88(C7): 4355–4367.
<https://dx.doi.org/10.1029/JC088iC07p04355>
- Rutherford R J, Herbert G J and Coffen-Smout S S. (2005). Integrated ocean management and the collaborative planning process: The eastern scotian shelf integrated management (ESSIM) initiative. *Marine Policy*, 29(1): 75–83.
<https://dx.doi.org/10.1016/j.marpol.2004.02.004>
- Shan S and Sheng J. (2012). Examination of circulation, flushing time and dispersion in Halifax Harbour of Nova Scotia. *Water Quality Research Journal of Canada*, 47(3–4): 353–374.
<https://dx.doi.org/10.2166/wqrjc.2012.041>
- Shan S, Sheng J, and Greenan B. (2014). Modelling study of three-dimensional circulation and particle movement over the Sable Gully of Nova Scotia. *Ocean Dynamics*, 64(1): 117–142.
<https://dx.doi.org/10.1007/s10236-013-0672-7>
- Sheng J. (2001). Dynamics of a buoyancy-driven coastal jet: The Gaspé current. *Journal of Physical Oceanography*, 31(11): 3146–3162.
[https://dx.doi.org/10.1175/1520-0485\(2001\)031<3146:DOABDC>2.0.CO;2](https://dx.doi.org/10.1175/1520-0485(2001)031<3146:DOABDC>2.0.CO;2)
- Sheng J, Greatbatch R and Wright D. (2001). Improving the utility of ocean circulation models through adjustment of the momentum balance. *Journal of Geophysical Research*, 106(106): 16711–16728.
<https://dx.doi.org/10.1029/2000jc000680>
- Sheng J, Zhao J and Zhai L. (2009). Examination of circulation, dispersion, and retention in Lunenburg Bay of Nova Scotia using a nested-grid circulation model. *Journal of Marine Systems*, 77(3): 350–365.
<https://dx.doi.org/10.1016/j.jmarsys.2008.0.1.013>
- Smagorinsky J. (1963). General circulation experiments with the primitive equations. *Monthly Weather Review*, 91(3): 99–164.
- Smith P C. (1992). Validation procedures for oil spill trajectory models. *Canadian Technical Report of Hydrography and Ocean Sciences*, 140: 168–183.
- Soomere T, Viikmäe B, Delpêche N, et al. (2010). Towards identification of areas of reduced risk in the Gulf of Finland, the Baltic Sea. *Proceedings of the Estonian Academy of Science*, 59(59): 156–165.
<https://dx.doi.org/10.3176/proc.2010.2.15>
- Taylor G. (1922). Diffusion by continuous movements. *Proceedings of the London Mathematical Society*, 2(1–4): 196–212.

- <https://dx.doi.org/10.1112/plms/s2-20.1.196>
- Tang C L. (1980). Mixing and circulation in the northwestern Gulf of St. Lawrence: A study of a buoyancy-driven current system. *Journal of Geophysical Research*, 85(C5): 2787–2796.
<https://dx.doi.org/10.1029/JC085iC05p02787>
- Tang L, Sheng J, Hatcher B G, et al. (2006). Numerical study of circulation, dispersion, and hydrodynamic connectivity of surface waters on the Belize shelf. *Journal of Geophysical Research*, 111(C1): 311–330.
<https://dx.doi.org/10.1029/2005JC002930>
- Thompson K R and Sheng J. (1997). Subtidal circulation on the Scotian Shelf: Assessing the hindcast skill of a linear, barotropic model. *Journal of Geophysical Research*, 102(1022): 24987–25004.
<https://dx.doi.org/10.1029/97JC00368>
- Thompson K R, Loucks R H and Trites R W. (1988). Sea surface temperature variability in the shelf-slope region of the Northwest Atlantic. *Atmosphere-Ocean*, 26(2): 282–299.
<https://dx.doi.org/10.1080/07055900.1988.9649304>
- Thompson K R, Dowd M, Shen Y, et al. (2002). Probabilistic characterization of tidal mixing in a coastal embayment: A Markov chain approach. *Continental Shelf Research*, 22(11–13): 1603–1614.
[https://dx.doi.org/10.1016/S0278-4343\(02\)00024-9](https://dx.doi.org/10.1016/S0278-4343(02)00024-9)
- Thompson K R, Ohashi K, Sheng J, et al. (2007). Suppressing bias and drift of coastal circulation models through the assimilation of seasonal climatologies of temperature and salinity. *Continental Shelf Research*, 27(9): 1303–1316.
<https://dx.doi.org/10.1016/j.csr.2006.10.011>
- Tseng R S. (2002). On the dispersion and diffusion near estuaries and around islands. *Estuarine, Coastal and Shelf Science*, 54(1): 89–100.
<https://dx.doi.org/10.1006/ecss.2001.0830>
- Urrego-Blanco J and Sheng J. (2012). Numerical investigation of interannual variability of circulation and hydrography over the eastern Canadian shelf. *Atmosphere-Ocean*, 50(3): 277–300.
<https://dx.doi.org/10.1080/07055900.2012.680430>
- Urrego-Blanco J and Sheng J. (2014a). Study on subtidal circulation and variability in the Gulf of St. Lawrence, Scotian Shelf and Gulf of Maine using a nested-grid coupled ocean-ice model. *Ocean Dynamics*, 64(3): 385–412.
<https://dx.doi.org/10.1007/s10236-013-0688-z>
- Urrego-Blanco J and Sheng J. (2014b). Formation and distribution of sea ice in the Gulf of St. Lawrence: A process-oriented study using a coupled ocean-ice model. *Journal of Geophysical Research*, 119(10): 7099–7122.
<https://dx.doi.org/10.1002/2014JC010185>
- Van der Baaren A and Prinsenber S. (2000a). Satellite-tracked ice drifter tests for accuracy and positioning, 1997–1998. *Canadian Technical Report of Hydrography and Ocean Sciences*, 209: vii + 47 p.
- Van der Baaren A and Prinsenber S. (2000b). Labrador shelf and gulf of St. Lawrence sea ice program, 1995–1998. *Canadian Technical Report of Hydrography and Ocean Sciences*, 207: vii + 213 p.
- Van der Baaren A and Prinsenber S. (2001). Satellite-tracked ice drifter program, 1999–2001. *Canadian Technical Report of Hydrography and Ocean Sciences*, 214: x + 88 p.
- Van der Baaren A and Prinsenber S. (2006). Wind forcing of ice drift in the southern gulf of St. Lawrence: Satellite-tracked ice drifter program 2004. *Canadian Technical Report of Hydrography and Ocean Sciences*, 245: xvii + 188 p.
- Van der Baaren A and Tang C L. (2009). Satellite-tracked surface drifter program: Scotian shelf 2007 and the Gulf of St. Lawrence 2008–2009. *Canadian Data Report of Hydrography and Ocean Sciences*, 183: ix + 80 p.
- Wang P and Sheng J. (2016). A comparative study of wave-current interactions over the eastern Canadian shelf under severe weather conditions using a coupled wave-circulation model. *Journal of Geophysical Research*, 121: 5252–5281.
<https://dx.doi.org/10.1002/2016JC011758>
- Weatherall P, Marks K M, Jakobsson M, et al. (2015). A new digital bathymetric model of the world's oceans. *Earth and Space Science*, 2(8): 331–345.
<https://dx.doi.org/10.1002/2015EA000107>
- Wu Y, Tang C and Hannah C. (2012). The circulation of eastern Canadian seas. *Progress in Oceanography*, 106(8–9): 28–48.
<https://dx.doi.org/10.1016/j.pocean.2012.06.005>